Lithographically fabricable, optimized three-dimensional solar cell random structure

2013 J. Opt. 15 105007

(http://iopscience.iop.org/2040-8986/15/10/105007)

IOP PUBLISHING JOURNAL OF OPTICS
J. Opt. **15** (2013) 105007 (7pp) doi:10.1088/2040-8978/15/10/105007

Lithographically fabricable, optimized three-dimensional solar cell random structure

Albert S Lin, Yan-Kai Zhong, Sze-Ming Fu, Chi-Wei Tseng, Shih-Yun Lai and Wei-Ming Lai

Institute of Electronic Engineering, National Chiao-Tung University, Hsinchu, 30010, Taiwan

E-mail: hdtd5746@gmail.com (A S Lin)

Received 16 May 2013, accepted for publication 12 August 2013
Published 3 September 2013
Online at stacks.iop.org/JOpt/15/105007

Abstract
The optimized random reflector is highly preferred for solar cells due to its superiority over an un-optimized totally random surface and its potential to exceed the Lambertian limit. There are some obstacles to overcome for realizing optimized random reflectors, including the feasibility from the process viewpoint and the intensive computational demand for large-scale random reflector design. Here a binary random grating is proposed which can be easily fabricated using common lithographic techniques. By using a global optimization algorithm and three-dimensional (3D) EMW simulation, the solar cell structure with 4×4 quasi-random binary grating can provide 23% higher integrated absorbance than its periodic grating counterpart and 103.5% higher integrated absorbance than a planar cell, approaching the Lambertian limit. Broad-band transmission improvement at short wavelength and a broad-band waveguiding effect at long wavelength is observed for the optimized 3D geometry. Additionally, the optimized random grating surpasses the periodic grating at all incident angles. The absorbance of the large-scale, fully optimized binary pattern can potentially exceed the Lambertian limit while its computational demand is shown to be manageable.

Keywords: Lambertian limit, random texture, quasi-guided mode, thin-film solar cell

(Some figures may appear in colour only in the online journal)

1. Introduction

Random reflectors are always of particular interest for solar cells. The optimized random geometry can potentially exceed the so-called Lambertian limit [1–12]. There are several issues associated with optimized random geometry. (1) The optimized random profiles are usually very difficult to fabricate. (2) The randomized nature means that the geometrical construction of conformal layers is quite difficult. A suitable geometrical definition of such a full 3D structure is needed if the solar cell geometry is to be optimized by a particular optimization algorithm. The geometry has to be adjusted automatically during optimization, rather than adjusted manually at each run. (3) A full three-dimensional (3D) solar cell structure with a random back reflector, a dielectric spacer, a conformal semiconductor layer, and a front-side anti-reflection coating has not been optimized to date due to its large computational demand.

Here a global optimization algorithm together with a geometrical parameterization procedure is proposed for designing optimal random gratings for future thin-film photovoltaics. There are several potential methods for global optimization, and the genetic algorithm (GA) is selected here due to its versatility and the fact that it does not require initial guesses. The proposed method can be applied to solar cells using any material although silicon thin-film is used in this study. In the literature, optimization of the one-dimensional (1D) randomized profile for solar cells has been reported [13, 14] using 2D simulation. In those works the optimized 1D profile proved difficult to fabricate, and two-dimensional

(2D) grating geometry in three-dimensional (3D) simulation is much preferred in real devices due to its higher absorbance enhancement. The initial result of this work can be found in [15].

2. Simulation methodology and the definition of random binary mask

The calculation is carried out by rigorously coupled wave analysis (RCWA). The absorbance is calculated by integrating the power dissipation in the silicon region:

$$A(\lambda) = \frac{\frac{1}{2}\int_V \omega\varepsilon_0\varepsilon''(\lambda)\left|\vec{E}(\vec{r})\right|^2 \mathrm{d}v}{\frac{1}{2}\int_S \mathrm{Re}\left\{\vec{E}(\vec{r})\times\vec{H}^*(\vec{r})\right\}\cdot \mathrm{d}\vec{s}} \quad (1)$$

where ω is the angular frequency, λ is the free space wavelength, ε_0 is the permittivity in vacuum, and ε'' is the imaginary part of the complex semiconductor dielectric constant. Only the absorption in silicon generates electron–hole pairs that contribute to photocurrent. In order to compare the light trapping capability of different structures, the integrated absorbance can be defined by integrating (1) weighted by solar spectrum:

$$A_{\mathrm{Int}} = \frac{\int \frac{\lambda}{hc}\Omega(\lambda)A(\lambda)\,\mathrm{d}\lambda}{\int \frac{\lambda}{hc}\Omega(\lambda)\,\mathrm{d}\lambda}, \quad (2)$$

where $\Omega(\lambda)$ is the AM 1.5 solar spectrum, h is the Planck constant, λ is the free space wavelength and c is the speed of light. Using integrated absorbance weighted by AM 1.5 spectrum, as stated in (2), is a common practice in the literature to compare the optical properties of solar cells [16, 17]. A global optimization algorithm is applied to conduct geometry optimization for random reflectors. A GA or an evolutionary algorithm is a stochastic global search method that mimics a natural biological evolution [18]. The principle of survival of the fittest is applied to a population of individuals, which are potential solutions to the problem. Individuals with higher fitness in the problem domain have better chance to be selected and to reproduce their own offspring. This results in individuals who are better suited to the environment tending to have more children and higher fitness as the evolution process proceeds, just as in natural adaptation. GAs are particularly suited for search in very large or unbounded sample spaces, and they have been proven useful in different fields [19–22]. Due to the fact that the current study is on quasi-random 4 × 4 binary mask, the search space is not very large and therefore the optimal solution by GA is very likely to be the global maximum. The structure for evolution should be defined in such a way that no matter how the random binary mask is evolved, the subsequent silicon and ZnO conformal coverage can be adjusted according to the underlying binary random pattern on the bottom ZnO layer. This is a complicated process and the description is included below.

The evolutionary structure consists of ZnO/Si/ZnO/Ag, the thickness of silicon is 700 nm, the thickness of layer 2 is 100 nm, and the groove height for the grating is 250 nm. The binary grating can be fabricated using usual lithography techniques in one etch step. Each binary bit is 250 nm in both width and length. The structure is defined using seven layers as illustrated in figure 1. Layer 1 is a uniform Ag layer. Layer 2 is a uniform ZnO layer. Layer 3 is a ZnO/Si layer, which is defined according to the binary mask pattern as a function of 0 and 1, as shown in figure 2.

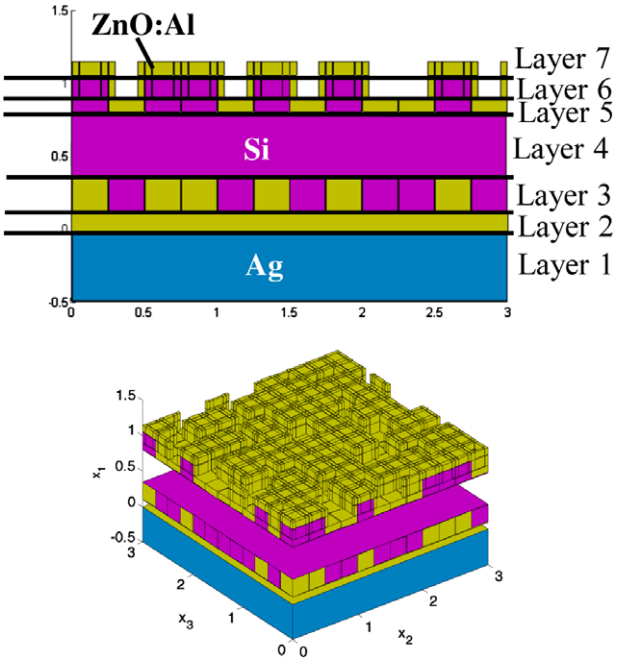

Figure 1. (Top) Cross section of layers and (bottom) 3D view.

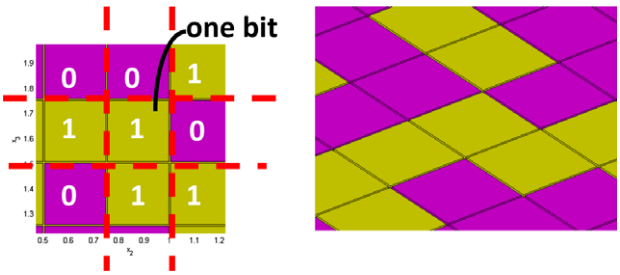

Figure 2. (Left) Illustration of the method to define layer 3 ZnO/Si and (right) 3D view.

The algorithm can be defined as below for layer 3:

$$\begin{aligned} &\textit{if} && \textbf{the binary mask is 1} \\ &&& \boldsymbol{n_{\mathrm{r}} = n_{\mathrm{ZnO}}} \\ &\textit{else if} && \textbf{the binary mask is 0} \\ &&& \boldsymbol{n_{\mathrm{r}} = n_{\mathrm{Si}}}. \end{aligned} \quad (3)$$

1 represents the mesa and 0 represents the etched area. Therefore in (3), 1 represents ZnO while 0 represents silicon since the etched region will be conformally filled with silicon. Afterward, layer 4 is a uniform layer of silicon, whose thickness will be the total thickness minus the groove depth of the grating. Layer 5 is silicon/ZnO, and the initial binary mask can be used to define the fifth layer. Layer 5 is part of the ZnO top contact conformal coverage.

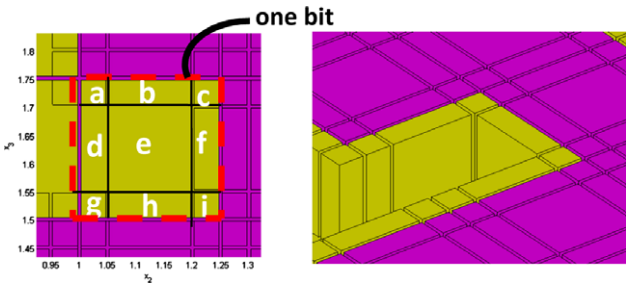

Figure 3. (Left) Illustration of the method to define layer 6 sidewall and (right) 3D view.

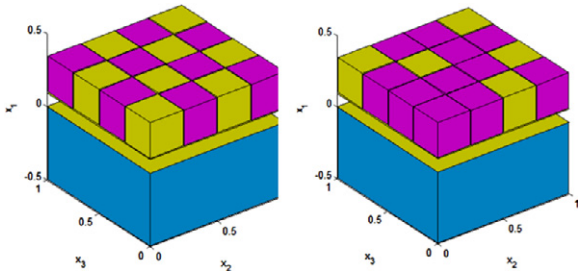

Figure 4. Left: periodic two-dimensional grating. Right: optimized quasi-random 4 × 4 grating.

Layer 6, which is the sidewall of the top silicon grating structure, is more complicated to define. The thickness of the sidewall is 50 nm, which is assumed to be half of the film thickness of the topmost ZnO coverage. As illustrated in figure 3, the side wall definition can be done by dividing one bit of binary mask pattern into nine sub-regions. Whether each sub-region should be air, silicon or ZnO is determined by whether its adjacent region is silicon or air and whether the underlying binary mask bit is 0 or 1. In addition, for each sub-region, the situation can be slightly different as stated below.

For the case of sub-regions a, b, c, d, f, g, h, or i, if the underlying binary mask bit is 1, a ZnO grating bump is already defined in the layer 3 at this specific mask bit location. Thus, in order to achieve conformal coverage, the silicon refractive index is used. In the case that the underlying binary mask bit is 0, which means at this specific mask bit location a ZnO grating dip is already defined in layer 3, the sub-region in the layer 6 should be air or ZnO, depending on whether any of the adjacent regions is silicon or not. If any of the adjacent regions is silicon then the ZnO refractive index is used since the sub-region in this case should be the ZnO sidewall of the adjacent silicon material:

$$\begin{aligned} &\textit{if} \quad \textbf{the binary mask is 1} \\ &\qquad n_{\mathrm{r}} = n_{\mathrm{Si}} \\ &\textit{else} \\ &\quad \textit{if} \quad \textbf{one of the adjacent region is silicon} \\ &\qquad\qquad n_{\mathrm{r}} = n_{\mathrm{ZnO}} \\ &\quad \textit{else} \\ &\qquad\qquad n_{\mathrm{r}} = n_{\mathrm{air}}. \end{aligned} \tag{4}$$

For sub-region e, the situation is simpler. If the underlying binary mask bit is 1, which means a ZnO grating bump is already defined in this specific mask bit location in layer 3, the silicon refractive index is used to construct the conformal coverage of the silicon thin-film. Otherwise, if the mask bit is 0, the air refractive index is used:

$$\begin{aligned} &\textit{if} \quad \textbf{the binary mask is 1} \\ &\qquad n_{\mathrm{r}} = n_{\mathrm{Si}} \\ &\textit{else} \\ &\qquad n_{\mathrm{r}} = n_{\mathrm{air}}. \end{aligned} \tag{5}$$

Layer 7 is the topmost ZnO front contact coverage, which constitutes part of the top ZnO conformal coverage. The thickness of the layer 7 ZnO coverage is 100 nm. The definition can be extended from layer 6 using the same sub-region method as depicted in (4) and (5). Material optical constants can be found in the literature [9, 23–29].

3. Spectral response and transmission

For the calculation of Poynting vector, energy loss, and integrated quantum efficiency, see [3, 13, 30, 31]. The calculated integrated absorbance, A_{Int}, is 0.7380 for the optimized geometry and 0.5697 for its periodic counterpart. The optimized grating geometry is shown in figure 4. The spectral response is shown in figure 5 where a 4 × 4 quasi-random grating provides 23% broad-band improvement compared to its 2D periodic counterpart. At short wavelength, the optimized structure shows broad-band improvement due to the transmission enhancement, as is clear in the inset of figure 5. At long wavelengths, the Fabry–Perot type resonances are seen in the 2D periodic grating due to the quasi-guided mode excitations.

The Lambertian absorption limit is [32]

$$A(\lambda) = \frac{(1 - \mathrm{e}^{-4\alpha W})}{[1 - (1 - 1/n^2)\mathrm{e}^{-4\alpha W}]}, \tag{6}$$

where α is the absorption coefficient, n is the semiconductor refractive index, and W is the film thickness. Although at the resonance frequencies the absorbance of the baseline cell with 2D periodic gratings can exceed the Lambertian limit in (6) at certain wavelengths, the broad-band enhancement is not as strong as the optimized random structure. The well-defined quasi-guided modes in the periodic grating make it possible to exceed the Lambertian limit. Nonetheless, at wavelengths other than the resonances, the absorbance is much lower. Since it is difficult for guided modes to exist over the entire solar spectrum, a compromised but optimized random grating can provide higher overall efficiency. The planar cell in general shows wave interference characteristics at the short wavelength where peak absorbance is seen when wave impedance is matched for the thin-film solar cell stack. It shows weak absorption at long wavelength due to insufficient light scattering, resulting from the lack of large angle diffraction.

The transmission at the solar cell front surface is plotted in the insets of figure 5. When calculating the transmittance, only the front surface texture is retained (no

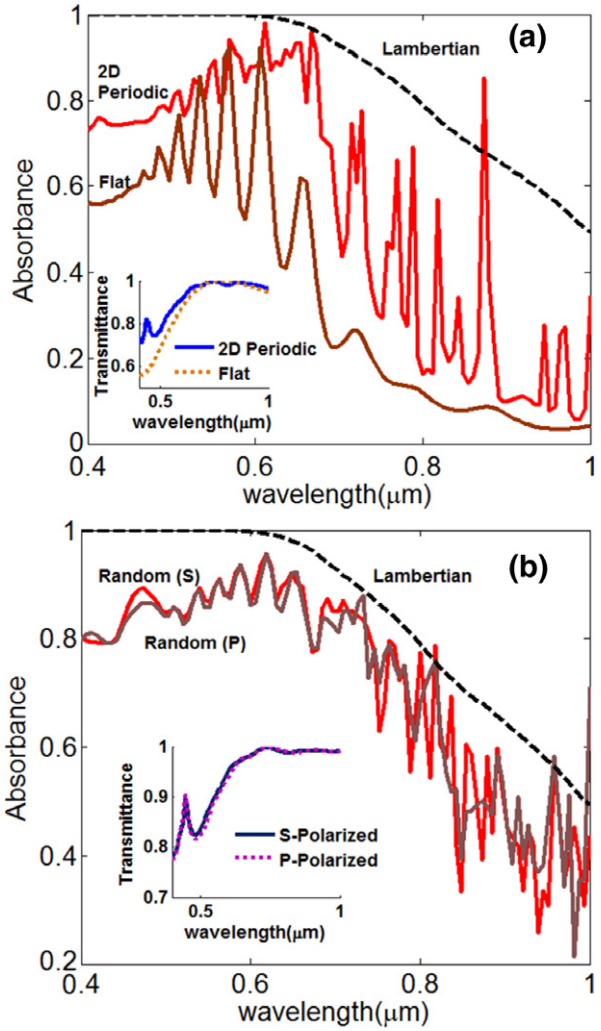

Figure 5. Spectral responses for (a) the 2D periodic grating and (inset) the transmission at the front surface and (b) the optimized 4 × 4 quasi-random grating and (inset) transmission at the front surface.

back reflector) and the fraction of the power penetrating from air into silicon is plotted. Retaining only the front surface texture is a common practice for calculating anti-reflection characteristics [33]. Since there is no back reflector, no quasi-guided mode is excited and therefore in the transmittance curve very few peaks are observed. At the long-wavelength portion of the solar spectrum, the transmission is essentially very high due to the matched wave impedance. The impedance-matched condition for the ZnO front contact assuming planar structure is

$$t_{\mathrm{ZnO}} = \frac{\lambda}{4n_{\mathrm{ZnO}}} + \frac{m\lambda}{2n_{\mathrm{ZnO}}}, \tag{7}$$

where λ is the free space wavelength, n_{ZnO} is the ZnO refractive index, and m is non-negative integer. For the 2D periodic grating the transmission is further improved at all wavelengths where a broad-band transmission is observed instead of perfect transmission at a single wavelength, as is the case for the planar structure. The lower transmission at the short wavelength for both insets in figures 5(a) and (b) is due to two factors. The first is directly from (7): n_{ZnO} is approximately equal to 2 and $t_{\mathrm{ZnO}} = 100$ nm, and thus the first impedance-matched point is around $\lambda = 800$ nm, and the second is $\lambda = 266.67$ nm. Since there is no impedance-matched point around $\lambda = 400$–600 nm, the transmission is lower at short wavelength. The second reason is that the imaginary part of dielectric constant ($\varepsilon_{\mathrm{r}}''$) becomes higher at short wavelength, which in turn lowers the transmission. The transmission peak around $\lambda = 448.5$ nm is unlikely to be the result of impedance matching since there is no such points in this spectral range. It is more likely due to the strong waveguiding effect where the ridged-geometry guides the incident wave into the silicon slab. The further broad-band transmission improvement of the random grating over the 2D periodic grating is due to its optimized geometry.

4. Angular response

Figure 6 illustrates the angular dependence of the integrated absorbance for the solar cells with 2D periodic grating or the optimized random grating. The angular variation of integrated absorbance is similar to that reported in the literature [27], where a small variation in absorbance for angles <50° and a significant drop of absorbance for larger incident angles are observed. The solar cell with the optimized random reflector shows higher integrated absorbance than its 2D periodic counterpart at all incident angles, despite the fact that the optimization here is with respect to the normal incidence. The optimization is done for normal incidence due to the fact that this is the incidence angle resulting in maximal power generation. It should be pointed out that optimization can also be done with respect to any angle or for an angle-averaged absorbance. The guided-mode excitation wavelengths in general shift with incidence angle for the 2D periodic grating, and the guided-mode excitation for random structures is less pronounced, similar to the situation for normal incidence.

The guided-mode excitation condition is when inplane incident wavevectors, after being augmented by grating momentum, coincide with the wavevector of eigen modes [34]:

$$\begin{aligned} k_{\mathrm{InPlane}} \pm G_x \pm G_y &= k_0 \sin(\theta_{\mathrm{i}}) \pm \frac{2\pi m_x}{a_x} \pm \frac{2\pi m_y}{a_y} \\ &= k_{\mathrm{eigen}}(\omega), \end{aligned} \tag{8}$$

where k_0 is the free space wavevector, k_{InPlane} is the tangential component of k_0 relative to the film, G is the reciprocal lattice vector, a_x and a_y are the grating period in the x and y direction, θ_{i} is the photon incident angle, and m_x and m_y are non-negative integers. The condition stated in (8) is impossible to be fulfilled for a broad-band spectrum due to the fact that quasi-guide modes only exist at discrete wavelengths [35]. Since the quasi-guided mode excitation is difficult to exist over the entire spectral range especially for normal incidence, the random and optimized design is a compromise way to achieve highest total absorbance.

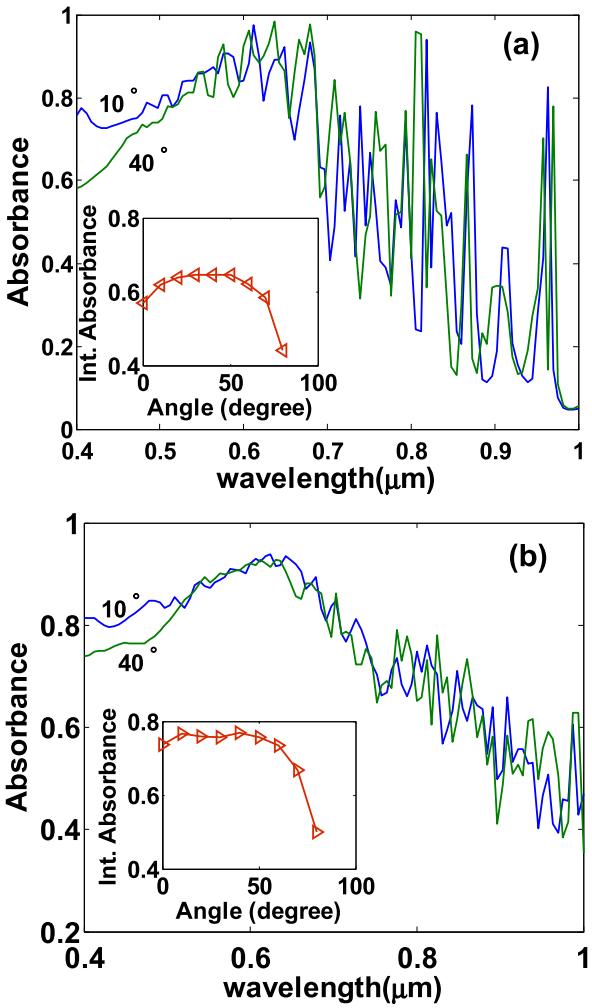

Figure 6. Spectral responses of S-polarized light for varying incidence angles for (a) 2D periodic grating and (inset) integrated absorbance versus angle and (b) optimized 4 × 4 quasi-random grating and (inset) integrated absorbance versus angle.

5. Computational consideration

It is certainly desirable to have a fully optimized random grating where an infinitely large mask pattern is optimized and thus the diffraction is the most efficient. In reality, an infinite large mask optimization is not necessary since the fringing effect will become negligible for a sufficient large mask pattern. This is true if the mask dimension is much larger than the wavelength so that the diffraction and interference at the fringe become unimportant. Two factors further reduce the mask size required to achieve a fully optimized, large-scale pattern. One is the absorption nature of the solar cell material where the field intensity decays exponentially as it propagates. The second is that the wavelength is shorter in semiconductors than in air. The order of Fourier components that needs to be retained is proportional to the dimension of binary random mask. From the inset of figure 7, for 4 × 4 quasi-random mask design, the Fourier component retained should be at least seven in order to have a convergent solution. Therefore, for 40 × 40 quasi-random mask design, it will take 70 diffraction orders if the same fine features still need to be resolved in a large-dimension mask pattern. This is evident from [36, 37]

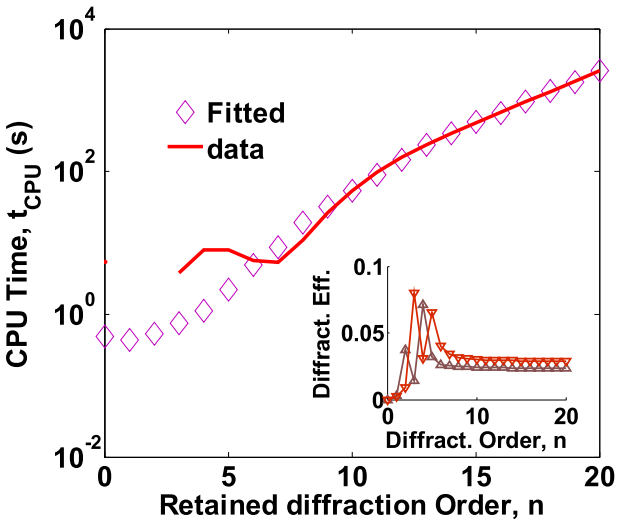

Figure 7. CPU time versus retained diffraction order. Inset: the required diffraction order for convergence.

Table 1. Parameters for polynomial fit.

Coefficient	p_1	p_2	p_3	p_4	p_5	p_6	p_7
Value	0.000 59	0.029 62	0.5827	−5.173	20.56	−29.17	5.475

$$\varepsilon(x) = \sum_n a_n \exp(\mathrm{j}k_n x) = \sum_n a_n \exp\left(\mathrm{j}\frac{2\pi n}{\Lambda}x\right), \quad (9)$$

where ε is periodic permittivity function, Λ is the period of grating, k_n is the wavevector of Fourier expansion, and n is diffraction order. It is clear from (9) that the number of required diffraction orders increases with the period Λ. From figure 7, 70 diffraction orders will take around 1.02 years to complete, using polynomial extrapolation formula fitted with data within 20 diffraction orders [38]:

$$t_{\mathrm{CPU}} = p_1 n^6 + p_2 n^5 + p_3 n^3 + p_4 n^4 + p_5 n^2 + p_6 n + p_7. \quad (10)$$

Table 1 lists the coefficients of the polynomial fit equation in (10). Clearly, in order to have a fully optimized mask design, cluster parallelization is essential. For example, if a cluster of 1000 CPU is running in parallel, it only takes 8.95 h to finish the above-mentioned computation. Although this still seems to be an extended time, it is certainly worth this CPU time since a fully optimized pattern can be re-used indefinitely.

6. Conclusion

The algorithm-optimized solar cell structure with 2D randomized grating in 3D simulation domain is reported in this work. The proposed binary random grating can be easily fabricated using common lithography techniques.

The optimized solar cell geometry with 2D quasi-random grating shows broad-band transmission enhancement for the high-energy photons, and broad-band waveguiding effect for the low-energy photons. The spectral response of the optimized structure shows less significant quasi-guided mode excitation but a higher total integrated absorbance for the AM 1.5 solar spectrum. The angular response of the optimized structure surpasses its periodic counterpart in all incident angles. This indicates that using random reflectors to achieve a compromised response over the full spectral range can lead to higher total absorptivity, compared to the periodic structures which rely on the high-Q quasi-guided mode excitations. The presented geometry parameterization, encoding, evolution, and global optimization procedures can be applied to large-scale, fully optimized random reflector pattern design, whose light trapping capability can potentially exceed the Lambertian limit. The CPU runtime for optimizing the large-scale random grating is shown to be manageable based on the polynomial extrapolation from the data within 20 diffraction orders.

References

[1] Yablonovitch E 1982 Statistical ray optics *J. Opt. Soc. Am.* **72** 899–907

[2] Ganapati V, Miller O D and Yablonovitch E 2012 Spontaneous symmetry breaking in the optimization of subwavelength solar cell textures for light trapping *Proc. 38th IEEE Photovoltaic Specialists Conf. (Austin)* 001572–001576

[3] Bhattacharya P 2006 *Semiconductor Optoelectronic Devices* 2nd edn (Upper Saddle River, NJ: Prentice-Hall)

[4] Hegedus S S and Kaplan R 2002 Analysis of quantum efficiency and optical enhancement in amorphous Si p–i–n solar cells *Prog. Photovolt., Res. Appl.* **10** 257–69

[5] Krc J, Smole F and Topic M 2003 Potential of light trapping in microcrystalline silicon solar cells with textured substrates *Prog. Photovolt., Res. Appl.* **11** 429–36

[6] Munuera C, Zuniga-Perez J, Rommeluere J F, Sallet V, Triboulet R, Soria F, Munoz-Sanjose V and Ocal C 2004 Morphology of ZnO grown by MOCVD on sapphire substrates *J. Cryst. Growth* **264** 70–8

[7] Sai H, Kanamori Y, Arafune K, Ohshita Y and Yamaguchi M 2007 Light trapping effect of submicron surface textures in crystalline Si Solar Cells *Prog. Photovolt., Res. Appl.* **15** 415–23

[8] Shah A, Torres P, Tscharner R, Wyrsch N and Keppner H 1999 Photovoltaic technology: the case for thin-film solar cells *Science* **285** 692–8

[9] Shah A, Schade H, Vanecek M, Meier J, Vallat-Sauvain E, Wyrsch N, Kroll U, Droz C and Bailat J 2004 Thin-film silicon solar cell technology *Prog. Photovolt., Res. Appl.* **12** 113–42

[10] Stiebig H, Schulte M, Zahren C, Haase C, Rech B and Lechner P 2006 Light trapping in thin-film silicon solar cells by nano-textured interfaces *Proc. SPIE* **6197** 619701

[11] Söderström T, Haug F-J, Terrazzoni-Daudrix V and Ballif C 2008 Optimization of amorphous silicon thin film solar cells for flexible photovoltaics *J. Appl. Phys.* **103** 114509

[12] Green M A, Emery K, King D L, Hishikawa Y and Warta W 2007 Solar cell efficiency tables (Version 29) *Prog. Photovolt., Res. Appl.* **15** 35–40

[13] Lin A and Phillips J D 2008 Optimization of random diffraction gratings in thin-film solar cells using genetic algorithms *Sol. Energy Mater. Sol. Cells* **92** 1689–96

[14] Sheng X, Johnson S G, Michel J and Kimerling L C 2011 Optimization-based design of surface textures for thin-film Si solar cells *Opt. Express* **19** A841–50

[15] Lin A, Fu S-M and Zhong Y-K 2012 Lithographically-definable solar cell random reflector using genetic algorithm optimization *Proc. 38th IEEE Photovoltaic Specialists Conf. (Austin)* 003030–003034

[16] Lin H-Y, Kuo Y, Liao C-Y, Yang C C and Kiang Y-W 2012 Surface plasmon effects in the absorption enhancements of amorphous silicon solar cells with periodical metal nanowall and nanopillar structures *Opt. Express* **20** A104–18

[17] Min C, Li J, Veronis G, Lee J-Y, Fan S and Peumans P 2010 Enhancement of optical absorption in thin-film organic solar cells through the excitation of plasmonic modes in metallic gratings *Appl. Phys. Lett.* **96** 133302

[18] Chipperfield A, Fleming P, Pohlheim H and Fonseca C 1994 *Genetic Algorithm Toolbox User Guide* (Sheffield: University of Sheffield)

[19] Preblea S, Lipson M and Lipson H 2005 Two-dimensional photonic crystals designed by evolutionary algorithms *Appl. Phys. Lett.* **86** 061111

[20] Deken B, Pekarek S and Dogan F 2006 Minimization of field enhancement in multilayer capacitors *Comput. Mater. Sci.* **37** 401–9

[21] Lipson H and Pollack J B 2000 Automatic design and manufacture of robotic lifeforms *Nature* **406** 974–7

[22] Shen L, Ye Z and He S 2003 Design of two-dimensional photonic crystals with large absolute band gaps using a genetic algorithm *Phys. Rev.* B **68** 035109

[23] Khoshman J M and Kordesch M E 2007 Optical constants and band edge of amorphous zinc oxide thin films *Thin Solid Films* **515** 7393–9

[24] Kang S J and Joung Y H 2007 Influence of substrate temperature on the optical and piezoelectric properties of ZnO thin films deposited by rf magnetron sputtering *Appl. Surf. Sci.* **253** 7330–5

[25] Ferlauto A S, Ferreira G M, Pearce J M, Wronski C R, Collins R W, Deng X and Ganguly G 2004 Analytical model for the optical functions of amorphous semiconductors and its applications for thin film solar cells *Thin Solid Films* **455/456** 388–92

[26] Optical Society of America 1994 *Handbook of Optics, Vol. 2: Devices, Measurements, and Properties* 2nd edn, vol 2, ed M Bass (New York: McGraw-Hill)

[27] Fragala M E, Malandrino G, Giangregorio M M, Losurdo M, Bruno G, Lettieri S, Amato L S and Maddalena P 2009 Structural, optical, and electrical characterization of ZnO and Al-doped ZnO thin films deposited by MOCVD *Chem. Vapor Depos.* **15** 327–33

[28] Kim H, Pique A, Horwitz J, Murata H, Kafafi Z, Gilmore C and Chrisey D 2000 Effect of aluminum doping on zinc oxide thin films grown by pulsed laser deposition for organic light-emitting devices *Thin Solid Films* **377/378** 798–802

[29] Elam J W, Routkevitch D and George S M 2003 Properties of ZnO/Al_2O_3 alloy films grown using atomic layer deposition techniques *J. Electrochem. Soc.* **150** G339–47

[30] Comsol AB 2006 *Comsol Multiphysics RF Module User Guide V 3.3* (Burlington, MA: COMSOL Inc)

[31] Synopsys 2005 *Sentaurus Device EMW User Manual V. X-2005.10* (Mountain View, CA: Synopsys)

[32] Green M A 2002 Lambertian light trappingin textured solar cells and light-emitting diodes: analytical solutions *Prog. Photovolt., Res. Appl.* **10** 235–41

[33] Paetzold U W, Moulin E, Pieters B E, Carius R and Rau U 2011 Design of nanostructured plasmonic back contacts for thin-film silicon solar cells *Opt. Express* **19** A1219–30

[34] Ghaemi H F, Thio T, Grupp D E, Ebbesen T W and Lezec H J 1998 Surface plasmons enhance optical transmission through subwavelength holes *Phys. Rev.* B **58** 6779–82
[35] Battaglia C *et al* 2012 Light trapping in solar cells: can periodic beat random? *ACS Nano* **6** 2790–7
[36] Moharam M G and Gaylord T K 1986 Rigorous coupled-wave analysis of metallic surface-relief gratings *J. Opt. Soc. Am.* A **3** 1780–7
[37] Moharam M G and Gaylord T K 1981 Rigorous coupled-wave analysis of planar-grating diffraction *J. Opt. Soc. Am.* **71** 811–8
[38] Royston P 2008 *Multivariable Model—Building: A Pragmatic Approach to Regression Anaylsis based on Fractional Polynomials for Modelling Continuous Variables* (New York: Wiley)